A Defocused and Cross-Pol-optimized Array-Fed Reflector Antenna Concept for Spaceborne SAR Applications

Sigurd Huber, Gerhard Krieger, Alberto Moreira, German Aerospace Center (DLR), Germany, sigurd.huber@dlr.de

Abstract

Spaceborne synthetic aperture radar (SAR) applications follow a trend whereupon increased swath width and finer resolution at longer wavelength are demanded. These requirements pose a challenge to future SAR antenna architectures and, subsequently, the radar instruments. To this day most SAR satellites employ active phased array antennas. However, the need of large antenna apertures renders planar arrays uncomfortable in terms of mass, size and cost. A promising alternative may be found in array-fed reflector antennas, which have been in use for satellite communications for decades. The obvious advantage of unfurlable reflectors lies in the provision of large apertures, whereas the feed array complexity is confined in a relatively small volume. This paper addresses some design challenges encountered, when adopting array-fed reflector antennas for spaceborne SAR sensors. One challenge is to preserve the functionality of the SAR system in case of a failure of a feed element, which usually results in a severe gain drop in a particular direction. To deal with this effect, an approach which could be called 'feed array defocusing' is presented. Another problem associated with array-fed reflectors are increased cross-polar levels. As low cross-polar levels are crucial for SAR polarimetry, here, an innovative azimuth beam shaping concept is introduced, which allows reducing cross-polar patterns and simultaneously suppressing the sidelobes of the azimuth antenna patterns. In order to quantify these cross-polar levels a performance figure is provided.

1 Introduction

Several countries around the world are involved in present and future Earth observation missions employing large orbital platforms. A notable number of these SAR systems undergo a change in terms of their antenna architecture from direct radiating planar arrays [7] towards large deployable mesh reflectors fed by arrays of feed elements [4, 6, 9, 1, 8]. This is especially true for missions that operate at L- and P-band frequencies and therefore require large apertures in order to maintain a sufficient sensitivity. A large receiving aperture is in particular required for wide-swath high-resolution missions where the available power is distributed over a wide angular domain in range and in azimuth.

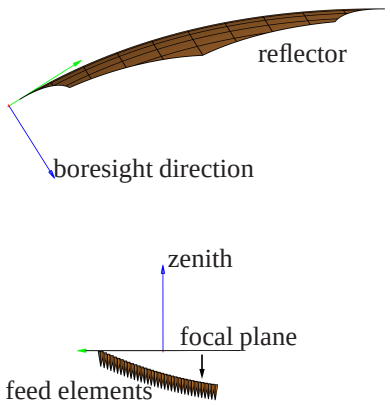

Figure 1: Array-fed reflector in an azimuth projection. Here, defocusing of the individual beams is achieved by shifting the feed elements away from the focal plane.

Reflector based antennas, however, have some inherent disadvantages compared to planar arrays. Illuminating a reflector with a set of feed elements means, that the reflected field is focused in a beam which basically does not overlap with the beam of an adjacent feed radiator. As consequence of this principle, array-fed reflectors usually sustain a severe gain drop in the direction associated with a dropped out feed element. In [3, 2] concepts based on reflector shaping are discussed which allow to reduce this gain drop effect. Another challenge is related to the fact that reflector antennas can generate much larger cross-polar fields, compared to direct radiating arrays, even if the primary illuminator (the feed element) is almost cross-polarization free. These secondary cross-polarized fields are induced by the scattering effects of an incident field on the reflector surface which result in a rotation of the polarization plane. Distinct cross-polar patterns manifest themselves in so called cross-talk in polarimetric SAR acquisitions. In the following, a feed array concept is discussed which optimizes the system performance with respect to these reflector-specific peculiarities.

2 Feed Array Defocusing

The basic principle of an array-fed SAR system can be illustrated at the example of Fig. 1. Here, only the reflector faced by an array of feed elements is drawn. The reflector and feed elements would be connected to the SAR satellite bus. In this configuration the SAR satellite would illuminate a swath located on the lower right edge of Fig. 1 (centered around the boresight direction).

Important to mention here is that the feed array is extended in this projection inside the paper plane, which is the flight direction (azimuth) of the SAR sensor. Typically, the feed elements are located in the focal plane of the reflector. The focal plane contains the focal point of a parabolic reflector (axis of revolution is the boresight axis) and as such is the place where feed elements will produce the narrowest possible beam[1].

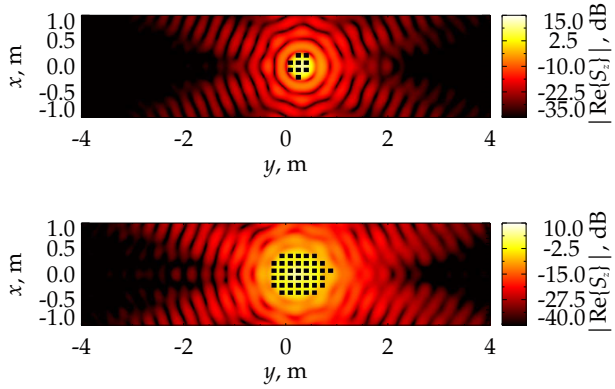

Figure 2: Upper image: Field distribution in the focal plane due to a plane wave arriving from a direction close to boresight. Lower image: Here, the field has been computed offset by 1 m to the focal plane. The defocusing effect requires now several more feed elements (indicated by the black patches) in order to collect the same amount of field energy.

An equivalent view on this problem is to look at the field distribution in the focal plane which is generated by a plane wave falling onto the reflector, say for example from boresight direction. This situation is depicted in the upper image of Fig. 2 where the z-component of the Poynting vector has been plotted as function of elevation (y-axis) and azimuth (x-axis) inside the focal plane. The position $(x, y) = (0, 0)$ is precisely the location of the focal point. The black patches symbolize feed elements collecting a certain amount of field power. In the lower image the same plane wave has been simulated, except that the field plane has been shifted away from the focal plane by 1 m. Evidently, now several more feed elements are required to collect the same amount of power as in the upper case. This comparison suggests that a defocused feed array is much less prone to feed element failures since adjacent elements still collect a large part of the incident field energy.

3 Azimuth Feed Array Concept

Most SAR systems under investigation for current and near-future missions still employ a single azimuth channel. Although, digitizing individual azimuth channels would allow for more sophisticated imaging concepts [4] with ultra-fine azimuth resolution, here, the purpose of the multiple feed elements in azimuth is solely to collect the spread-out field energy. Further, dual polarized feed elements are considered, since driving requirements for future SAR missions are polarimetric capabilities.
The basic concept here is to form a weighted sum of the individual ports (h: horizontal polarization, v: vertical polarization) of the feed elements as schematically illustrated in Fig. 3. If, for example, a h-polarized beam shall be formed, then the magnitude of the even-numbered weights w will be small compared to the uneven-numbered weights. The main purpose of the even-numbered weights in this case is to suppress the cross-polar fields. On the other hand the uneven-numbered weights mainly serve producing a sharp co-polar beam with desirably low sidelobes in azimuth.

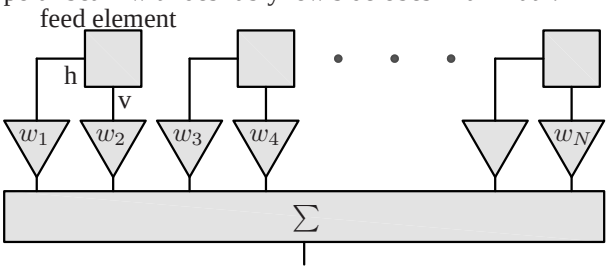

Figure 3: Azimuth feed array concept. N dual polarized feed element ports are combined via a fixed-weight beamforming network. This feed element group represents a single elevation element (or channel) in the entire feed array.

This can be formulated as a constrained optimization problem according to [5]

$$\begin{aligned} \text{minimize} \quad & \boldsymbol{w}^{\mathsf{H}} \boldsymbol{R}_{\boldsymbol{v}} \boldsymbol{w} && (1) \\ \text{subject to} \quad & \boldsymbol{w}^{\mathsf{T}} \boldsymbol{a}_{\mathrm{co}}(\boldsymbol{k}_0) = 1 && (2) \\ & |\boldsymbol{w}^{\mathsf{T}} \boldsymbol{a}_{\mathrm{co}}(\boldsymbol{k}_{\mathrm{SL},i})|^2 \leq \eta_{\mathrm{SL}} && (3) \\ & |\boldsymbol{w}^{\mathsf{T}} \boldsymbol{a}_{\mathrm{cx}}(\boldsymbol{k}_{\mathrm{cx},j})|^2 \leq \eta_{\mathrm{cx}} \, . && (4) \end{aligned}$$

Expression (1) represents the total noise power, with noise channel covariance matrix $\boldsymbol{R}_{\boldsymbol{v}}$ and equation (2) is a constraint maximising the beam in the direction of the wavenumber $\boldsymbol{k}_0$. In this context $\boldsymbol{a}_{\mathrm{co}}$ describes the so called array manifold, with the co-polar patterns as its elements. Correspondingly, $\boldsymbol{a}_{\mathrm{cx}}$ represents the cross-polar array manifold in equation (4). The solution to this optimization problem is known as *minimum variance distortionless response* (MVDR) beamforming in the literature [10]. The additional constraints (3) and (4) are for sidelobe control and cross-pol rejection. Here, the indices i and j indicate that the wavenumber domain corresponding to the sidelobes $\boldsymbol{k}_{\mathrm{SL},i}$ and the cross-polar maxima $\boldsymbol{k}_{\mathrm{cx},j}$ is discrete for the numerical optimization problem.

4 Performance Evaluation

In order to bear a reference to a real scenario, Germany's Tandem-L mission proposal [6] shall serve as demonstration example. The Tandem-L satellites will orbit Earth in

[1] This is only approximately true. In reality the place for a most focused beam and a given direction might lie on a fairly complicated surface.

a height of 740 km and acquire single- and dual-polarized data over a swath width of 350 km starting at an incident angle of 26.3 ° and quad-pol images over a reduced swath width of 175 km. The geometrical dimensions of the reflector antenna are summarized in Table 1. As shown in Fig. 1, one way to defocus the feed elements is to shift

frequency	1.2575 GHz
azimuth diameter	15 m
elevation diameter	15 m
focal length	13.5 m
offset (elevation)	9 m
azimuth elements	8
azimuth spacing	0.6 λ
elevation elements	39
elevation spacing	0.6591 λ
feed array size	6.13 m $\times$ 1.26 m

Table 1: Physical parameters defining an example of a defocused array-fed reflector.

them away from the focal plane. In this example the feed elements have been placed on a quadratic surface, where the elements on the right side have been shifted by 1.6 m in the negative nadir direction. Since the feed elements on the left side already experience sufficient defocusing they have been kept close to the focal plane. It is important to point out that there are potentially many other surfaces where feed elements may be placed in order to produce sufficient defocusing.

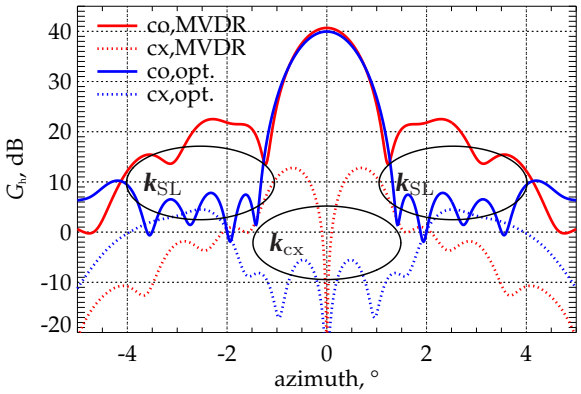

Figure 4: Azimuth gain pattern cuts corresponding to an elevation channel at the center of the feed array. The red curves correspond to the MVDR beamforming technique. In blue the optimized azimuth patterns, taking additional sidelobe and cross-polarization constraints into account, are shown.

Figure 4 shows an example of an optimized azimuth gain pattern

$$G = \frac{|\boldsymbol{w}^{\mathsf{T}}\boldsymbol{a}|^2}{\boldsymbol{w}^{\mathsf{H}}\boldsymbol{R}_v\boldsymbol{w}}\,, \tag{5}$$

in comparison to a simple MVDR beam. G in this example is a beam in the h-channel and the array manifold $\boldsymbol{a}$ refers either to the co- or the cross-polar pattern. $\boldsymbol{R}_v$ is assumed to be the identity matrix. These patterns correspond to a group of azimuth feed elements close to the center of the feed array. Note, this far field pattern is a so called secondary pattern, which is produced by the feed field scattered at the reflector. It should also be noted that the optimization has been performed using 2-D antenna patterns where the constraints may be taken anywhere in the azimuth-elevation plane. The beam is directed to $\boldsymbol{k}_0$ at azimuth angle zero degree while simultaneously suppressing the sidelobes close to the main beam and reducing the cross-polar levels in the Doppler domain of interest. In case of Tandem-L the Doppler domain roughly lies between azimuth angles $\pm 0.5\,°$.

The performance of this feed array concept in case of elevation channel drop outs can be evaluated by looking at Fig. 5. Important to mention is that with 'elevation channel' an entire group of azimuth feed elements as presented in Fig. 3 is meant. Behind the summation network would follow the T/R-module, an A/D converter and beamforming electronics. These are the components which would typically drop out and render the respective elevation channel unavailable for beamforming. Insofar in our example the feed array has 39 elevation channels (see Table 1).

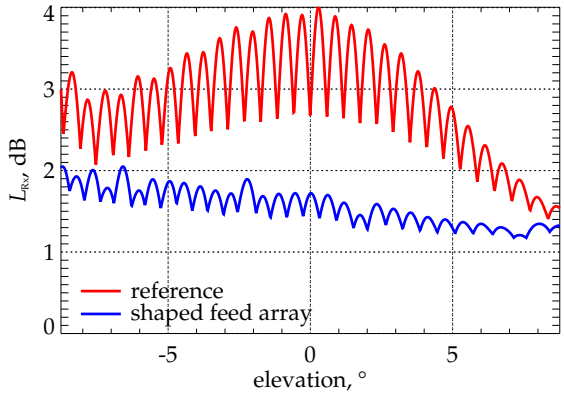

Figure 5: Loss patterns assuming a single failed elevation channel per direction. The reference refers to the case when all feed elements are placed in the focal plane (focused system), while the blue curve shows the effect of defocusing the feed elements as indicated in Fig. 1.

Figure 5 shows the loss in gain, with MVDR beamforming in elevation, when each of the 39 elevation channels drops out. The red curve represents the case of a 'focused' system where the feed elements are placed in the focal plane while the blue curve refers to the shaped feed array as shown in Fig. 1. The angular domain in elevation corresponds exactly to the 350 km swath intended for Tandem-L in single- and dual-polarization mode.

As pointed out above, quad-pol acquisitions rely on low cross-polar levels since they would contaminate the other polarization channel. Clearly, cross-talk in the 'hv'- and 'vh'-channel is most critical as the backscattered signal is weaker compared to co-polarized channels. A performance metric quantifying cross-talk may be derived from

the following polarimetric SAR signal model (for the ith elevation channel)

$$\begin{bmatrix} u_{\mathrm{hh}} & u_{\mathrm{hv}} \\ u_{\mathrm{vh}} & u_{\mathrm{vv}} \end{bmatrix}_i \sim \begin{bmatrix} r_{\mathrm{co,h}} & r_{\mathrm{cx,v}} \\ r_{\mathrm{cx,h}} & r_{\mathrm{co,v}} \end{bmatrix}_i \begin{bmatrix} s_{\mathrm{hh}} & s_{\mathrm{hv}} \\ s_{\mathrm{vh}} & s_{\mathrm{vv}} \end{bmatrix} \times \begin{bmatrix} t_{\mathrm{co,h}} & t_{\mathrm{cx,v}} \\ t_{\mathrm{cx,h}} & t_{\mathrm{co,v}} \end{bmatrix}_i + \begin{bmatrix} v_{\mathrm{h}} & v_{\mathrm{h}} \\ v_{\mathrm{v}} & v_{\mathrm{v}} \end{bmatrix}_i \quad (6)$$

The SAR signal u is proportional to the receive pattern r times a scattering coefficient s times the transmit pattern t superimposed by thermal receiver noise v (with noise covariance matrix $\boldsymbol{R}_v$). Applying digital beamforming coefficients $\boldsymbol{w}$ now in elevation, not to be confused with the beamforming coefficients in Fig. 3 which have been applied in azimuth, reveals the coupling of the individual patterns and the scattering coefficients.

$$u_{\mathrm{DBF,hh}} \sim \boldsymbol{w}^{\mathsf{T}}(\underline{\boldsymbol{r}_{\mathrm{co,h}} s_{\mathrm{hh}} t_{\mathrm{co,h}}} + \boldsymbol{r}_{\mathrm{cx,v}} s_{\mathrm{vh}} t_{\mathrm{co,h}} + \boldsymbol{r}_{\mathrm{co,h}} s_{\mathrm{hv}} t_{\mathrm{cx,h}} + \boldsymbol{r}_{\mathrm{cx,v}} s_{\mathrm{vv}} t_{\mathrm{cx,h}}) \quad (7)$$

$$u_{\mathrm{DBF,hv}} \sim \boldsymbol{w}^{\mathsf{T}}(\boldsymbol{r}_{\mathrm{co,h}} s_{\mathrm{hh}} t_{\mathrm{cx,v}} + \boldsymbol{r}_{\mathrm{cx,v}} s_{\mathrm{vh}} t_{\mathrm{cx,v}} + \underline{\boldsymbol{r}_{\mathrm{co,h}} s_{\mathrm{hv}} t_{\mathrm{co,v}}} + \boldsymbol{r}_{\mathrm{cx,v}} s_{\mathrm{vv}} t_{\mathrm{co,v}}) \quad (8)$$

Note, here the vector $\boldsymbol{r}$ represents the elevation array manifold on receive. The underlined term is the signal of interest which is superimposed by terms involving cross-polar patterns. The 'vh'- and 'vv'-signals are formed analogously. Then a ratio of the spectral power contained in the cross-talk terms and the signal power may be formulated according to equations (9) and (10). Here, h_{az} denotes the azimuth filter, which can for example perform Hamming weighting, as it is the case for Tandem-L. This ratio of cross-talk-to-signal shall be abbreviated $CTSR$

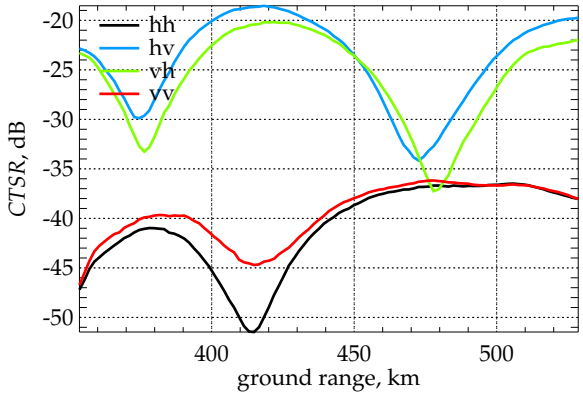

Figure 6: Cross-talk-to-signal ratio ($CTSR$) for the reflector with shaped feed array but without cross-pol cancellation.

in the following. Figures 6 and 7 show the cross-talk performance for quad-pol operation over a swath width of 175 km. In Fig. 6 the case is presented when no cross-pol cancellation is performed and for the sake of simplicity also no sidelobe control. This represents basically the simple MVDR beamformer in azimuth with expressions (1) and (2) while Fig. 7 shows the result with the full set of constraints. Here, a L-band shrubs backscatter model [11] has been assumed. Investigations showed that the $CTSR$ could be even worse for focused array-fed reflectors.

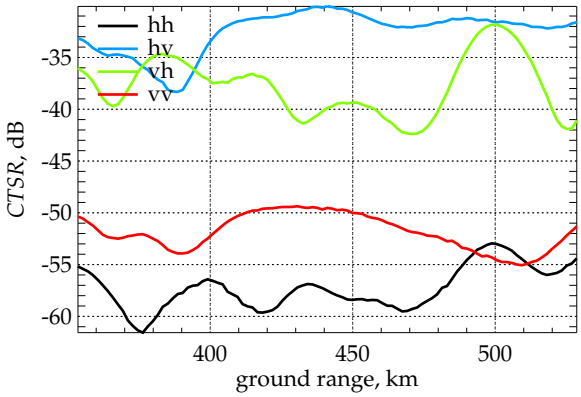

Figure 7: Cross-talk-to-signal ratio ($CTSR$) for the reflector with shaped feed array employing cross-pol cancellation.

5 Discussion and Conclusion

The feed array concept presented here attempts to serve several purposes. One is to maintain sufficient sensitivity under failure conditions. The above feed array design aims at single azimuth channel systems and as such requires one-dimensional defocusing methods which affect mainly the elevation direction. As shown for instance in [2] such an effect may be obtained by shaping the reflector surface adequately. But also hybrid approaches are thinkable where feed array and reflector are shaped in combination. Nevertheless, feed array defocusing could be interesting for multi-azimuth channel systems too, where a certain overlap between the azimuth channels (in terms of their respective patterns) may also prove beneficial with respect to the robustness of azimuth beamforming techniques. The reasoning behind this is that the dynamic range, within which the complex antenna patterns have to be known, decreases compared to focused systems.

A further issue tackled with a combined cross-polar and sidelobe rejection approach is to mitigate cross-talk effects in quad-pol SAR imagery. Here, eight dual polarized feed elements with a total of 16 antenna ports had been available. This approach could be expanded to the transmit case with much more feed elements involved and potentially produce even better results. As a side comment: For very wide swath and ultra-fine resolution SAR scenarios, the conception of vertical and horizontal polarization has to be taken with care. For instance a h-polarized wave emitted by the SAR sensor may be horizontally aligned in the frame of the SAR antenna, but it may no more be horizontally aligned on ground at large elevation and azimuth angles. This could be accounted for in this feed array architecture by individually setting constraints for each elevation channel.

$$CTSR_{\mathrm{hh}} = \frac{\int_{f_\mathrm{D}} |\boldsymbol{w}^\mathsf{T}(\boldsymbol{r}_{\mathrm{cx,v}} s_{\mathrm{vh}} t_{\mathrm{co,h}} + \boldsymbol{r}_{\mathrm{co,h}} s_{\mathrm{hv}} t_{\mathrm{cx,h}} + \boldsymbol{r}_{\mathrm{cx,v}} s_{\mathrm{vv}} t_{\mathrm{cx,h}}) h_{\mathrm{az}}|^2 \mathrm{d}f_\mathrm{D}}{\int_{f_\mathrm{D}} |\boldsymbol{w}^\mathsf{T} \boldsymbol{r}_{\mathrm{co,h}} s_{\mathrm{hh}} t_{\mathrm{co,h}} h_{\mathrm{az}}|^2 \mathrm{d}f_\mathrm{D}} \tag{9}$$

$$CTSR_{\mathrm{hv}} = \frac{\int_{f_\mathrm{D}} |\boldsymbol{w}^\mathsf{T}(\boldsymbol{r}_{\mathrm{co,h}} s_{\mathrm{hh}} t_{\mathrm{cx,v}} + \boldsymbol{r}_{\mathrm{cx,v}} s_{\mathrm{vh}} t_{\mathrm{cx,v}} + \boldsymbol{r}_{\mathrm{cx,v}} s_{\mathrm{vv}} t_{\mathrm{co,v}}) h_{\mathrm{az}}|^2 \mathrm{d}f_\mathrm{D}}{\int_{f_\mathrm{D}} |\boldsymbol{w}^\mathsf{T} \boldsymbol{r}_{\mathrm{co,h}} s_{\mathrm{hv}} t_{\mathrm{co,v}} h_{\mathrm{az}}|^2 \mathrm{d}f_\mathrm{D}} \tag{10}$$

The concept presented here offers some advantage over fully focused reflector antennas for SAR applications. Usually, optimizing a SAR antenna in one direction means sacrificing at another place. For example defocusing a reflector antenna always results in an increase of the feed array - this is the nature of defocusing. If the feed array is kept in size, defocusing will degrade the imaging performance mainly in terms of ambiguities. However, with a well balanced optimization approach, as introduced here, the potential benefits outweigh the disadvantages.

References

[1] F. Hélière, A. Carbone, J. G. N. Fonseca, N. Ayllon, A. Barnes, and M. Fehringer, "Biomass P-band SAR," in *11th European Conference on Synthetic Aperture Radar (EUSAR)*, Jun 2016, pp. 1–4.

[2] S. Huber, M. Younis, G. Krieger, and A. Moreira, "A Dual-Focus Reflector Antenna for Spaceborne SAR Systems with Digital Beamforming," *IEEE Transactions on Antennas and Propagation*, vol. 61, no. 3, pp. 1461–1465, 2013.

[3] S. Huber, M. Younis, G. Krieger, A. Moreira, and W. Wiesbeck, "A Reflector Antenna Concept Robust Against Feed Failures for Satellite Communications," *IEEE Transactions on Antennas and Propagation*, vol. 63, no. 4, pp. 1218–1224, Apr 2015.

[4] G. Krieger, S. Huber, M. Villano, F. Q. de Almeida, M. Younis, P. López-Dekker, P. Prats, M. Rodriguez-Cassola, and A. Moreira, "SIMO and MIMO System Architectures and Modes for High-Resolution Ultra-Wide-Swath SAR Imaging," in *11th European Conference on Synthetic Aperture Radar (EUSAR)*, Jun 2016, pp. 1–4.

[5] J. Liu, A. B. Gershman, Z.-Q. Luo, and K. M. Wong, "Adaptive Beamforming With Sidelobe Control: A Second-Order Cone Programming Approach," *IEEE Signal Processing Letters*, vol. 10, no. 11, pp. 331–334, Nov 2003.

[6] A. Moreira, G. Krieger, I. Hajnsek, K. Papathanassiou, M. Younis, P. Lopez-Dekker, S. Huber, M. Villano, M. Pardini, M. Eineder, F. D. Zan, and A. Parizzi, "Tandem-L: A Highly Innovative Bistatic SAR Mission for Global Observation of Dynamic Processes on the Earth's Surface," *IEEE Geoscience and Remote Sensing Magazine*, vol. 3, no. 2, pp. 8–23, Jun 2015.

[7] T. Motohka, Y. Kankaku, and S. Suzuki, "Advanced Land Observing Satellite-2 (ALOS-2) and its follow-on L-band SAR mission," in *IEEE Radar Conference (RadarCon)*, May 2017, pp. 0953–0956.

[8] J. R. Piepmeier, P. Focardi, K. A. Horgan, J. Knuble, N. Ehsan, J. Lucey, C. Brambora, P. R. Brown, P. J. Hoffman, R. T. French, R. L. Mikhaylov, E.-Y. Kwack, E. M. Slimko, D. E. Dawson, D. Hudson, J. Peng, P. N. Mohammed, G. D. Amici, A. P. Freedman, J. Medeiros, F. Sacks, R. Estep, M. W. Spencer, C. W. Chen, K. B. Wheeler, W. N. Edelstein, P. E. O'Neill, and E. G. Njoku, "SMAP L-Band Microwave Radiometer: Instrument Design and First Year on Orbit," *IEEE Transactions on Geoscience and Remote Sensing*, vol. 55, no. 4, pp. 1954–1966, Apr 2017.

[9] P. A. Rosen, Y. Kim, and V. R. Sagi, "Global Persistent SAR Sampling with the NASA-ISRO SAR (NISAR) Mission," in *IEEE Radar Conference (RadarCon)*, May 2017, pp. 0410–0414.

[10] H. L. V. Trees, *Optimum Array Processing*. John Wiley & Sons, Inc., 2002.

[11] F. T. Ulaby and M. Dobson, *Handbook of Radar Scattering Statistics for Terrain*. Artech House, Inc., 1989.